



Joint Institute for Nuclear
Research

SCIENCE BRINGING NATIONS TOGETHER



JOINT INSTITUTE FOR NUCLEAR RESEARCH

Frank Laboratory of Neutron Physics (FLNP)

FINAL REPORT ON THE START PROGRAMME

Investigation of Local Crystallographic
Texture in Silicified Fossil Wood by X-Ray
Diffraction

Supervisor

*Prof. Dmitry Nikolayev,
Department of Neutron Research
of Condensed Matter,
Frank Laboratory of Neutron
Physics (FLNP), JINR.*

Student

*Sancia Morris,
Department of Chemical
Engineering,
Institute of Chemical Technology,
Mumbai.*

Participation period

*February 11 – April 06
Winter Session 2024*

Dubna, Russia - 2024

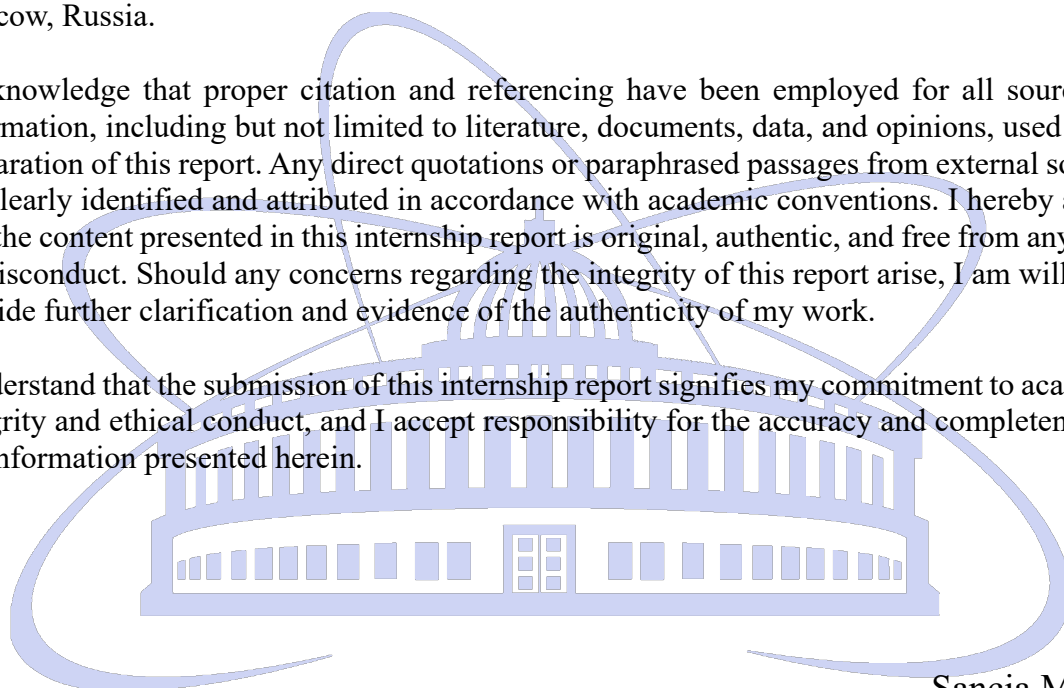
Declaration

I, **Sancia Morris**, hereby solemnly declare that the internship report entitled "**Investigation of Local Crystallographic Texture in Silicified Fossil Wood by X-Ray Diffraction**" is a genuine and original work carried out by me under the supervision of **Prof. Dmitry Nikolayev**, during my internship at the Department of Neutron Research of Condensed Matter, Frank Laboratory of Neutron Physics (FLNP), Joint Institute for Nuclear Research (JINR), Dubna, Moscow, Russia.

I assert that all the information presented in this report is the result of my own efforts and reflects my understanding and analysis of the tasks, projects, and experiences encountered during the internship period. Any contributions or assistance provided by others in the completion of this report have been duly acknowledged and credited in the acknowledgments section. It is entirely the product of my own research, observations, and reflections conducted within the organizational framework of Joint Institute of Nuclear Research (JINR), Dubna, Moscow, Russia.

I acknowledge that proper citation and referencing have been employed for all sources of information, including but not limited to literature, documents, data, and opinions, used in the preparation of this report. Any direct quotations or paraphrased passages from external sources are clearly identified and attributed in accordance with academic conventions. I hereby assure that the content presented in this internship report is original, authentic, and free from any form of misconduct. Should any concerns regarding the integrity of this report arise, I am willing to provide further clarification and evidence of the authenticity of my work.

I understand that the submission of this internship report signifies my commitment to academic integrity and ethical conduct, and I accept responsibility for the accuracy and completeness of the information presented herein.



Sancia Morris

Acknowledgements

I would like to express my sincere gratitude to Prof. Dmitry Nikolayev, Department of Neutron Research of Condensed Matter, Frank Laboratory of Neutron Physics (FLNP), Joint Institute for Nuclear Research (JINR), Dubna, Moscow, Russia, for his guidance, support, and valuable feedback throughout the duration of my internship. His expertise and encouragement significantly contributed to my learning and professional growth during this experience.

I am also grateful to Prof. Tatiyana Lychagina, for her valuable insights, support, and guidance complemented the mentorship, enriching my learning experience and contributing significantly to the success of this internship.

I am deeply thankful to the entire team at Joint Institute for Nuclear Research (JINR), for welcoming me to their institute and providing me with opportunities to engage in meaningful projects and tasks.

I would like to extend my appreciation to the staff and personnel of JINR for their assistance and cooperation during my internship. Their willingness to answer questions, offer guidance, and provide resources enhanced my understanding of the organization and its operations.

I would like to express my heartfelt gratitude to Ms. Elena Karpova. Her dedication, support, and coordination played a pivotal role in facilitating the seamless integration of interns into the institute's environment and ensuring the success of our internship experience. Her guidance and assistance in organizing orientation sessions, providing necessary resources, and addressing any concerns were instrumental in creating a conducive learning environment for all interns.

I also wish to thank my family and friends for their unwavering support, understanding, and encouragement during my internship experience. Their belief in my abilities motivated me to strive for excellence and persevere through challenges.

Lastly, I would like to acknowledge the countless individuals whose work, publications, and resources have enriched my understanding of the topics discussed in this internship report. Their contributions have been invaluable in shaping my perspective and informing my analysis.

This internship experience has been a rewarding and enriching journey, and I am grateful to all who have contributed to its success in various ways.

Publication Intent

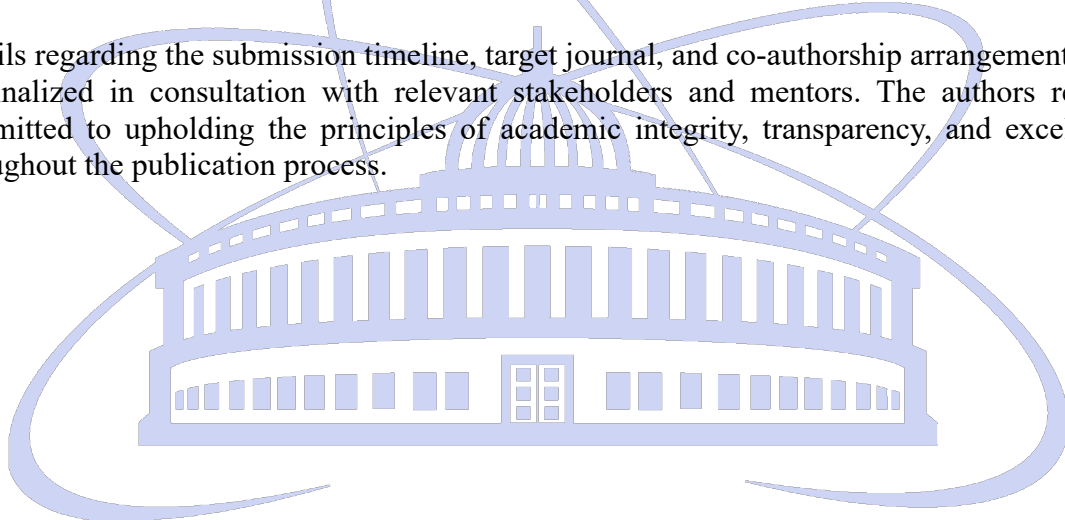
The research and findings documented in this internship report have been conducted with the aim of contributing to the scholarly discourse. It is the intention of the authors to disseminate this work through publication in a reputable peer-reviewed journal.

The insights, analyses, and conclusions drawn from the internship experience represent a valuable addition to the existing body of knowledge in the field. The rigorous research methodology employed, coupled with the practical application of theoretical concepts, has resulted in findings that hold significance for both academia and practitioners.

Efforts will be made to ensure that this work undergoes thorough peer review and meets the standards of academic excellence prior to publication. The authors are committed to engaging with the editorial process, addressing reviewer feedback, and refining the manuscript to ensure its scholarly rigor and contribution to the field.

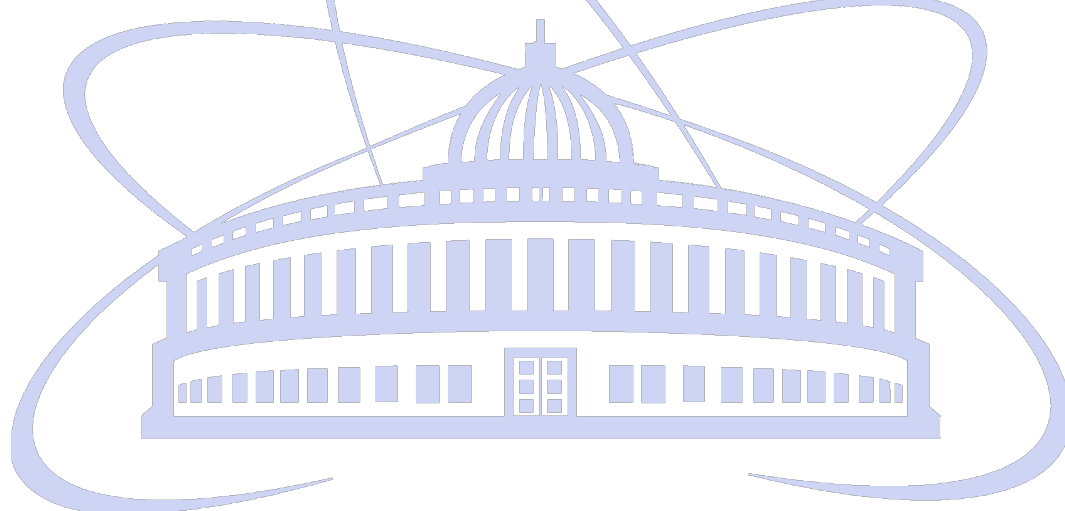
Publication of this work serves not only to showcase the achievements and contributions of the internship experience but also to foster dialogue, exchange of ideas, and further advancements in the respective field. The authors are eager to share their findings with the broader academic community and contribute to ongoing discussions and debates.

Details regarding the submission timeline, target journal, and co-authorship arrangements will be finalized in consultation with relevant stakeholders and mentors. The authors remain committed to upholding the principles of academic integrity, transparency, and excellence throughout the publication process.



Abstract

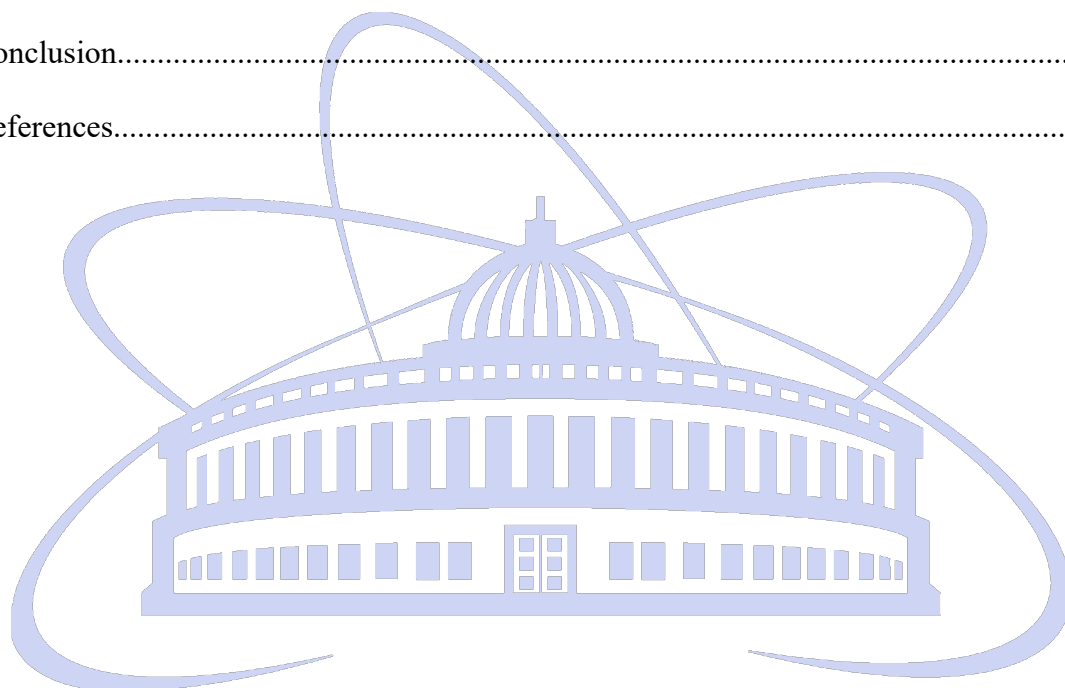
The discovery, compositional and anatomical study of silicified wood has been done extensively all around the world in great numbers. The classification of silicified wood as such deals with all forms and phases of silica that comes under its umbrella. One such class of silicified wood is fossil wood having a high content of quartz, and there are very limited mentions about this category of fossilized wood. A fresh approach to such samples is by studying the crystallographic texture of fossil wood to understand the orientation of crystals, replacing the organic matter within the sample. This work focuses on the crystallographic texture analysis based on measured pole figures. The intensity of the pole density maxima on pole figures measured on the center surface part of the analyzed samples is higher, then that on the edges. It affirms that the crystallographic texture is sharper at the center part compared to the less ordered texture at the edge. The X-ray tomography study, conducted to understand the difference of elemental distribution within the sample, reveals the more X-ray absorbing phase on the edge of both the samples, which leads to the difference in the intensity of the crystallographic texture. We believe that this research on silicified wood is the first research work, which encompasses crystallographic texture analysis with pole figures: an approach previously not undertaken in similar studies.



Contents

Abstract

1. Introduction.....	01
2. Materials and Methods.....	04
3. Results.....	08
3.1. XRD.....	08
3.2. XRT.....	11
4. Discussion.....	13
5. Conclusion.....	15
6. References.....	16



1. Introduction

Wood is a natural material that has been present on Earth's surface for several billions of years. Fossil wood plays a crucial role in paleontological and geological studies, providing valuable insights into ancient ecosystems and environmental conditions. Mustoe et al., (2022) emphasized the significance of Cenozoic fossil wood from Thailand in understanding past environments. Additionally, Clary & Wandersee (2012) discussed how petrified wood can enhance public understanding of geologic time and evolution. Silicified wood is rock formed with minerals containing silica substituting the organic material, which turned into a fossil over time by various processes. They form typically polycrystalline materials and can be composed of a single mineral or even different combinations of minerals. Many forms of fossilized wood, including petrified (Husien et al., 2021; Soomro et al., 2016), silicified (Tosal et al., 2023; Oktariani et al., 2019), pyritized (Dmitry), permineralized, and char wood, have been found all over the world from various eras like Late Pennsylvanian (Tosal et al., 2023; Mencl et al., 2009), Miocene (Soomro et al., 2016), Pliocene (Oktariani et al., 2019), Pleistocene (Jochems et al., 2022), Mesozoic-Cenozoic (Wang et al., 2006), Permian (Dietrich et al., 2013). These types of wood vary based on the location, the availability of specific materials, and the type of preservation that the wood has undergone. The discovery and study of this kind of fossilized wood have been the subject of numerous research projects, with the characterization and classification of the wood receiving most of the attention. Certain publications also delve into comprehending the sample's composition (Jochems et al., 2022), internal structure (Dietrich et al., 2013), pores (Husien et al., 2021), paleoenvironmental information (Tosal et al., 2023), and so on. Since fossilized wood has a distinct morphology and replaces organic material with minerals inside the newly formed rock structure, it is an intriguing category with a plethora of research potential.

Silicified fossil wood is a significant find in paleontological studies, providing insights into ancient ecosystems and environmental conditions. The process of silicification, where wood is replaced by silica, can preserve intricate details of the wood's structure and composition over millions of years (Trümper et al., 2018). Silicified wood has been discovered in various locations worldwide, such as the Pleistocene Touro Passo Formation in Brazil (Benício et al., 2016), the Cenomanian of Vienne in France (Boura et al., 2019), and the Miocene Bruneau Woodpile in Idaho, USA (Viney et al., 2017). These findings indicate the widespread occurrence of silicified wood across different geological periods.

Studies have shown that silicified wood can contain not only the wood structure but also other elements like fungi, foliage fossils, spores, pollen grains, and flowers, providing a more comprehensive view of past ecosystems (Harper et al., 2016). The presence of fungal hyphae in silicified wood is not uncommon in the fossil record, further highlighting the diverse interactions and preservation potential of silicified wood (Xie et al., 2023). Additionally, the chemical composition of silicified wood can be analyzed to determine its botanical origin, as seen in the Cupressaceae family from the Noto Peninsula in Japan (Ludwiczuk & Asakawa, 2015). Silicified wood has also been used in material science research, with studies mimicking the microstructure of natural silicified wood to create porous ceramics (Mizutani et al., 2005). Furthermore, the mineralogy of silicified wood specimens can be evaluated through density measurements, providing insights into the silicification process (Mustoe et al., 2020). Observations from volcanoclastic deposits, like those from Mount St. Helens, have contributed to understanding the burial and silicification processes of fossil forests (Karowe & Jefferson, 1987). One of these exciting research areas pertains to the way the wood is encased in the fossil

and how the crystals arrange around it in a particular orientation impacting the crystallographic texture of the formed fossilized wood. The orientation that the crystallites choose to arrange themselves in the matrix depends on how the wood influences the crystallites. This property may be utilized in the future to grow crystallites in the required orientation by using an appropriate organic matrix (Pakhnevich et al., 2023b). The organized crystal matrix around the wood can be investigated for their crystallographic texture since the wood contributes to this specific attribute of crystal arrangement.

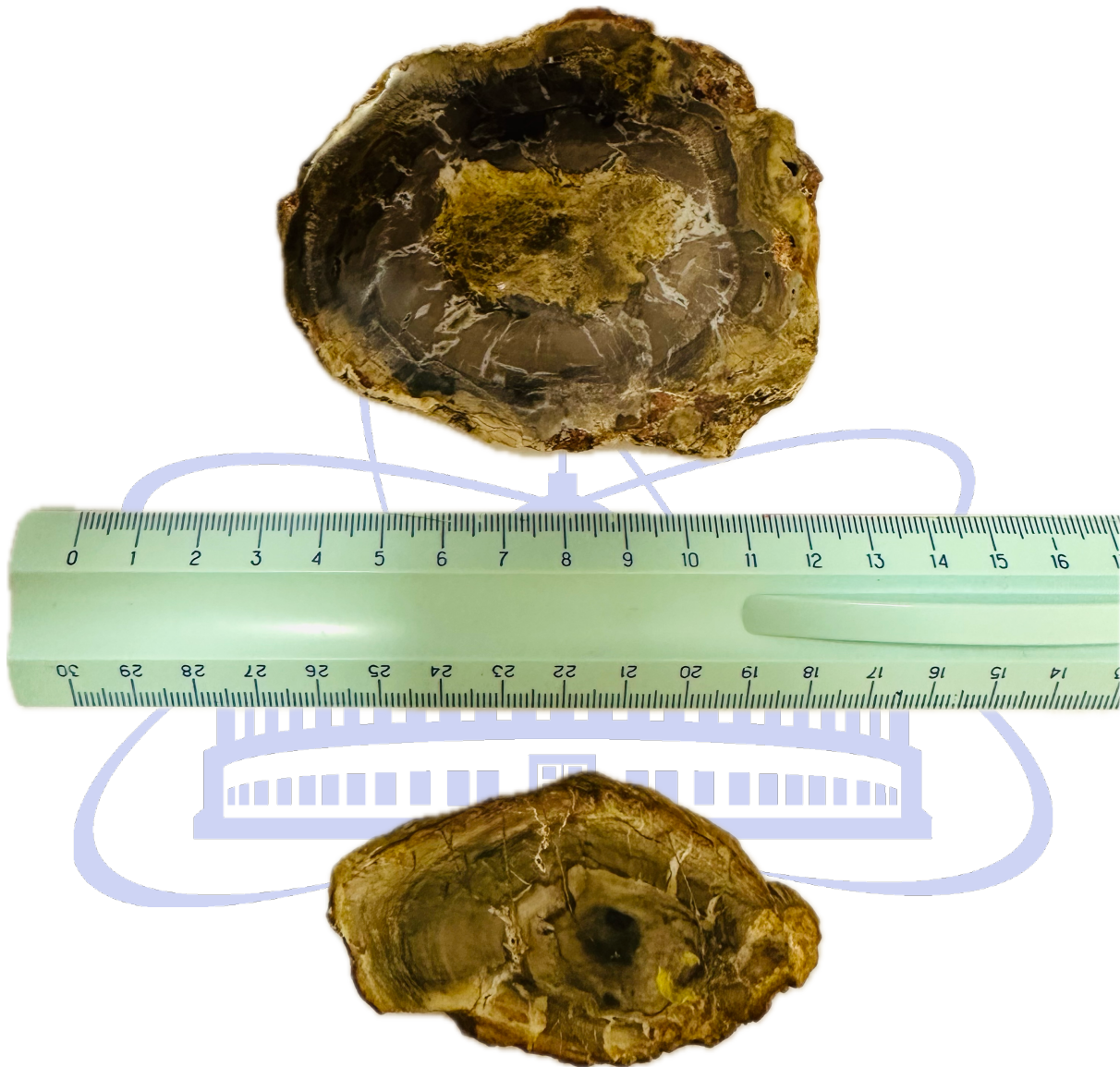
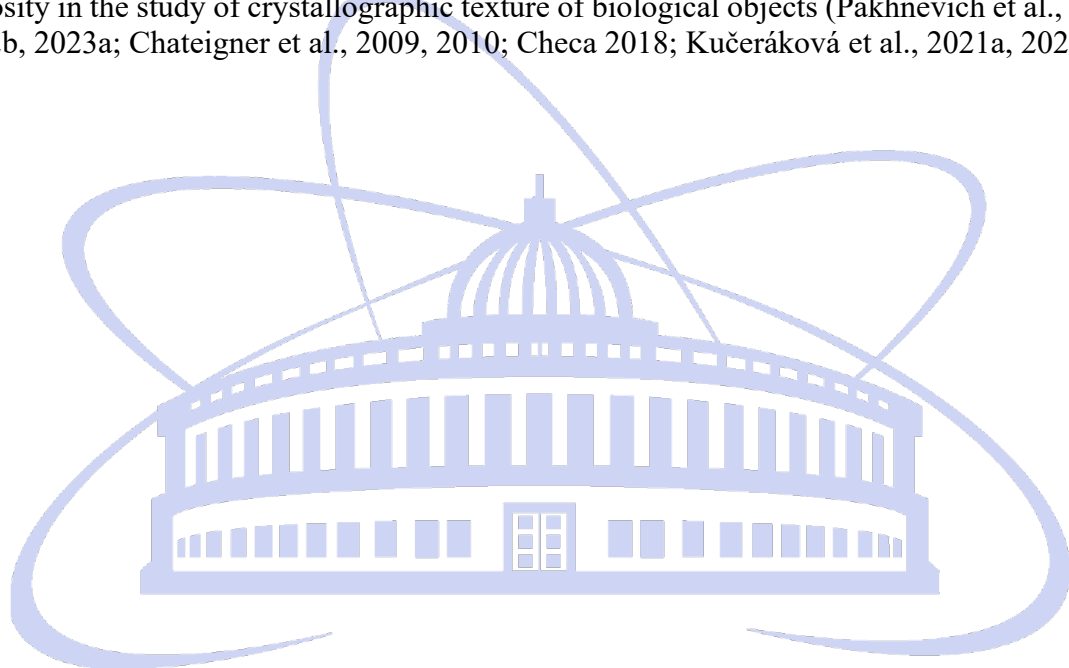


Figure 1 Silicified Wood Samples - Large and Small

Numerous studies and data exist regarding the identification and characteristics of silicified wood, which is primarily composed of silica or its various forms, such as quartz, quartz-silica, opal-A, opal-C, and so forth. The term "Silicified wood" refers to a broad category of fossilized wood that contains silica in all its forms and phases. Our study on silicified wood is based on the analysis of crystallographic texture on a piece of wood, fossilized by alpha quartz. It's also interesting that the majority of previous research on this kind of work has focused on reports of fossilized wood from various regions of the globe, such as Spain (Tosal et al., 2023), Borneo (Husien et al., 2021), Thailand (Wang et al., 2006), Germany (Dietrich et al., 2013), South

Africa (Yoon & Kim, 2008; Cairncross et al., 2020), Arizona (Sigleo, 1978), Czech Republic (Mencl et al., 2009) etc. Characterization studies, composition analysis, morphological (Soomro et al., 2016) structural, anatomical (Husien et al., 2021; Yoon & Kim, 2008), content analysis, defects etc. were also undertaken. There have been previous studies on silicified wood with Alpha-quartz crystallization reported by (Mencl et al., 2009; Matysova et al., 2008; Oktariani et al., 2019). This is one of the first observations with pole figure studies, even though studies have employed XRD for phase analysis (Jochems et al., 2022; Oktariani et al., 2019, Matysova et al., 2016; Kuczumow et al., 2000). There haven't been any prior record that emphasizes enough on crystallographic texture analysis on silicified wood samples that adequately describes the importance of the study in the field.

In the past, most of the crystallographic texture research focused primarily on metals and alloys (Bunge 1982; Bunge & Predehl 2002; Brokmeier 2006; Isaenkov et al., 2018, 2021; Stolbov et al., 2021; Wang et al., 2022; Lychagina et al., 2015, 2018; Lychagina & Brokmeier 2001; Ari-Gur et al., 2021; Ghosh et al., 2019; Hibino et al., 2021; Klosk, 2017; Nguyen-Minh et al., 2024; Tandon et al., 2024). However, in more recent times, there has been a great deal of curiosity in the study of crystallographic texture of biological objects (Pakhnevich et al., 2021, 2022b, 2023a; Chateigner et al., 2009, 2010; Checa 2018; Kučeráková et al., 2021a, 2021b).



2. Materials and Methods

The silicified wood samples from the Republic of Madagascar, which is located off the coast of Southeast Africa have been studied. Geologists were able to calculate the age of the samples, which comes from the Late Triassic. The wood samples, which have been recognized as fossilized wood with alpha quartz phase.

One of the most used tools for studying crystal phases, texture and structure is X-ray diffraction (XRD). By irradiating the sample with X-rays that do not damage it, diffraction is a non-invasive and non-destructive way to determine the crystal structure and texture. Following the observation of the intensity of the rays diffracted from the sample, the scattering angle of these rays is determined. By examining the diffracted peak's intensity and location, one can quickly ascertain the material's structure. To enable accurate XRD measurements, the samples were polished to have a smooth, flat surface. The X-ray diffraction study at $\lambda = 1.54\text{\AA}$ was carried out using Cu-K α radiation with the apparatus EMPYREAN from Malvern PANalytical, which is housed at the Frank Laboratory of Neutron Physics (FLNP) at the Joint Institute of Nuclear Research (JINR).

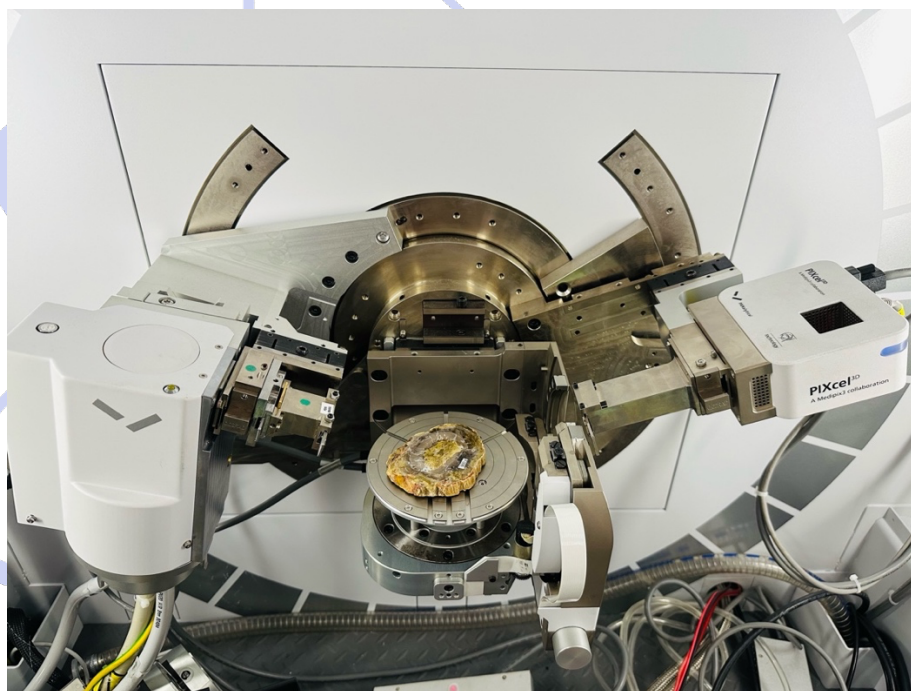


Figure 2 XRD Experimental Setup - MALVERN PANalytical EMPYREAN

The bulk sample with the smooth, flat surface was used for the measurements. It was set up on the sample holder and left in the course of the X-ray once it was emitted from the source and reflected onto the detector. A scan, carried out by adjusting the height of the sample holder with the sample, is crucial because it precisely ascertains the ideal height at which the best intensity of reflected light would occur. After determining the sample's necessary height—which is optimal for X-ray diffraction—a scan is conducted to assess the phases present in the sample prior to the X-ray measurements for the texture analysis. This is accomplished by using the PDF-2 database and the PANalytical HighScorePlus software package, version 4.1, which allows for the identification of the component present in the sample based on the results of the scan. A Ni filter was used to get rid of K β lines of the X-rays. The preliminary scan parameters

were a 10 mm mask, slits of 0.25° and 0.5° , a voltage of 40kV, a current of 40mA, and an exposure time of 300s per frame.

Pole figures, alternatively referred to as stereographic projections or pole plots, serve as visual aids in materials science and geology for illustrating the distribution of crystal orientations in each specimen. Their utility is especially evident in the examination of polycrystalline substances, including metals, minerals, and ceramics. Pole figures are plotted from the corrected and recalculated data obtained when the sample diffracts the X-rays incident from the source from X-ray diffraction, which are scattered by virtue of the atom's crystal arrangement and texture upon interaction with the electrons. Multiples of random distribution (mrd) is the term used to describe about the intensity of the samples measured. To represent intensity distributions resulting from random processes, multiples of random distributions are utilized. Multiples of random distribution for intensity representation involve adjusting the randomness of a distribution using a scaling factor k , where k is a positive real number. This technique allows for controlling the intensity levels while preserving the inherent randomness of the distribution. It provides a flexible method for modeling intensity variations in different phenomena across various disciplines. Whether applied in physics, materials science, or engineering, this approach serves as a versatile tool for understanding and characterizing variability in experimental outcomes. Researchers can tailor the intensity representation by adjusting the scaling factor k to meet specific experimental needs. This method finds extensive use in fields where randomness is a significant factor, facilitating the modeling and simulation of complex systems with realistic intensity fluctuations.

When measuring the pole figures of the crystallographic plane hkl , the 2θ value takes the value in accordance with Bragg's law for the reflection from this plane and is maintained constant. The rotation axes of the spatially oriented sample for analysis allow it to be rotated around two of the axes perpendicular to each other while maintaining one fixed axis (ω). The phi (ϕ) axis represents rotation around the vertical axis of the sample holder and is instrumental in examining orientations within the plane of the sample surface. The chi (χ) axis pertains to rotation around the horizontal axis of the sample holder. Chi (χ) scans are employed to explore orientations during sample tilting. The intensity of the reflected beam from the sample is measured at the detector present to collect the reflected rays.

During the XRD texture experiment, only incomplete pole figures up to an χ angle of 70° or 80° can be measured. The primary cause of this can be linked to the following issues. The sample's texture is measured for a predetermined, fixed area irradiated by the incident beam that hits the sample. The sample is rotated by an angle of 5° , and then at this position the reflected intensity is determined by counting for a given time equal 15 s in our case. This area stays the same until the sample is tilted from its initial position. However, once the sample is tilted from its starting angle, the pre-set area could change because of the sample's surface reflection path changing after the incident ray's path changes. This causes the area that the incoming rays irradiate to fluctuate and becomes inconsistent with each measurement, which causes variations in the reflected intensity that the detector records. This means that to make up for the intensity loss, some correction variables must be added. In order to correct for intensity loss at various angles of the tilted sample, the absorption correction factor is taken into account. Defocusing, which happens when the incoming ray reflects from the sample at low angles and causes problems with the sample's focusing, is another issue that arises frequently. With every variation in the sample's tilt angle, this impact serves as yet an additional trigger for permitting lower intensity levels. Because part of the defocusing problem needs to be addressed for the precise measurement of the sample parameters, the defocusing problem

cannot be fully controlled by altering the absorption adjustments alone. As a result, an intensity correction for defocusing is also necessary. This is downloaded from a database containing calculations or measurements-based corrections for non-textured materials at different tilting angles. When the tilt angle increases, defocusing causes the diffraction lines to become more broadly spaced. Since the defocusing adjustments do not yield improved results at tilt angles greater than 70°, the measurements must be stopped between 70° and 80°, yielding only partial pole numbers.

Based on the results of the 2θ scan recorded between 20° and 70°, it was found that the surface layer of the sample contains only one alpha quartz phase and the crystallographic planes (100), (110), (011), and (102) were selected for PF measuring. These specific planes were chosen because, in comparison to the other detected peaks, they had the highest reflected intensity and an appropriate signal to background ratio. Besides, these planes have simple Miller indices, which make PF measured for these planes convenient for interpretation. Since the reflection from the (006) plane was not recorded, the PF for this plane was recalculated using ODF reconstructed from other measured PFs. This method of the pole figure finding for the plane, reflection on which is typically not measured or not very intense was chosen since (006) is the typical plane for trigonal crystals and is hence one of the favored pole figures for interpretation. It took around 4h36min to measure the one pole figure for each crystallographic plane of the samples, and 12min to carry out the background measurements, requiring approximately 15s and 12s per step, respectively. The complete pole figures have been reconstructed using ODF from the measured pole figures using the WIMV (Matthies et al., 1987) approach (short for Williams (1968), Imhof (1982) and Matthies & Vinel (1982)) because the XRD only gives us incomplete pole figures. The program X'Pert Texture version 1.3 from PANalytical is used to calculate Orientation Distribution Function (ODF) and complete pole figures. (Nikolayev et al., 1999)

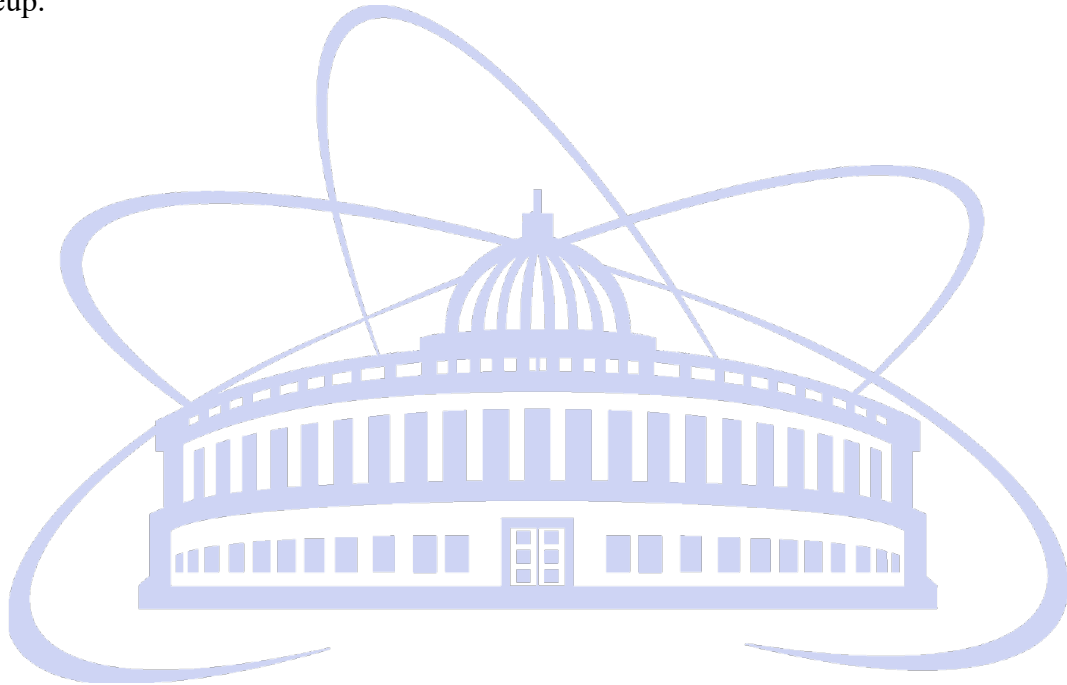
ODF is a three-dimensional probability density function that provides the volume of grains with a particular orientation in the sample. The 3D structure is essentially transformed into a 2D structure to compute and depict the ODFs as pole figures. Since the pole figures obtained from XRD are incomplete and only measured up to 70°, the ODF can be used to compute the complete pole figures because it contains complete information about crystallographic texture. Besides, ODF allows us to calculate pole figures, which are significant but challenging to measure because small peaks or poor signal-to-background ratios interfere with the observations. The ODF is computed using the corrected PFs with considering the defocusing. Pole figures are calculated from the ODF in such a way as to get the lowest possible value of Reciprocal Pole (RP) (Matthies, 1987). The Reciprocal Pole value serves as a quantitative metric to evaluate the agreement between recalculated pole figures and measured experimental data. It helps to assess how well the calculated crystallographic orientations align with actual observations. RP can be mathematically calculated as

$$RP = \sqrt{\frac{\sum_{i=1}^N (I_{measured,i} - I_{calculated,i})^2}{\sum_{i=1}^N I_{measured,i}^2}}$$

The incomplete pole figures are recalculated using the ODF to form complete pole figures as only these can be normalized. Once normalization is done, the maximum and minimum pole densities can be obtained from the measured sample area and studied. For a normalized pole figure, the following expression is valid:

$$\oint_{\gamma} P_h(y) dy = \int_0^{\pi} \sin \vartheta d\vartheta \int_0^{2\pi} d\varphi P_h(y) = 4\pi$$

The samples were mostly examined at the center and edge using XRD. Since X-rays do not have a very strong penetration power, most of the points measured were not very deep but rather only on the surface of the samples. To investigate the interior makeup of the samples, namely the minerals that make up the samples, X-ray tomography study was conducted. Using the XRT, it is also possible to see how the element present in the fossil affects the density and orientation of the crystals. With a three-dimensional representation of the sample's internal composition that forms the silicified wood and essentially highlighting element differences through distinct contrasts, XRT provides us with the element distribution. Every element has a unique X-ray absorption coefficient, which is reflected in the results by contrasting. If a mixture of elements is present in the sample, there will be different sets of contrast in the result. At the Joint Institute of Nuclear Research's (JINR) Frank Laboratory of Neutron Physics (FLNP), Prodis.NDT Micro Computerized Tomography was used to examine the samples' internal makeup.



3. Results

In this study, we employed XRT and XRD techniques to examine the elemental composition and crystallographic texture of silicified wood samples. The characterization of these samples is crucial for understanding their composition and texture. By analyzing the XRD diffraction patterns and XRT images, we aim to elucidate the phases and texture of the mineral matter present in the samples. These findings will contribute to a comprehensive understanding of the texture within the samples in a better way.

3.1 XRD

The XRD measurements and its subsequent analysis reveals that the primary constituent of the samples is alpha quartz. The sample has trigonal crystal system, and it was confirmed as the element quartz by comparing the initial scan data with the PDF-2 database for quartz, having the space group P3221 with number 154. The Reference code for quartz card in the PDF-2 database is 01-085-0930 with unit cell parameters $a = 4.9110\text{\AA}$, $b = 4.9110\text{\AA}$, and $c = 5.4070\text{\AA}$. The angles between them are $\alpha = 90^\circ$, $\beta = 90^\circ$ and $\gamma = 120^\circ$. The XRD patterns show the comparison of data obtained from the two samples and how the intensity varies when the area of measurement changes from the center of the samples to the edge.

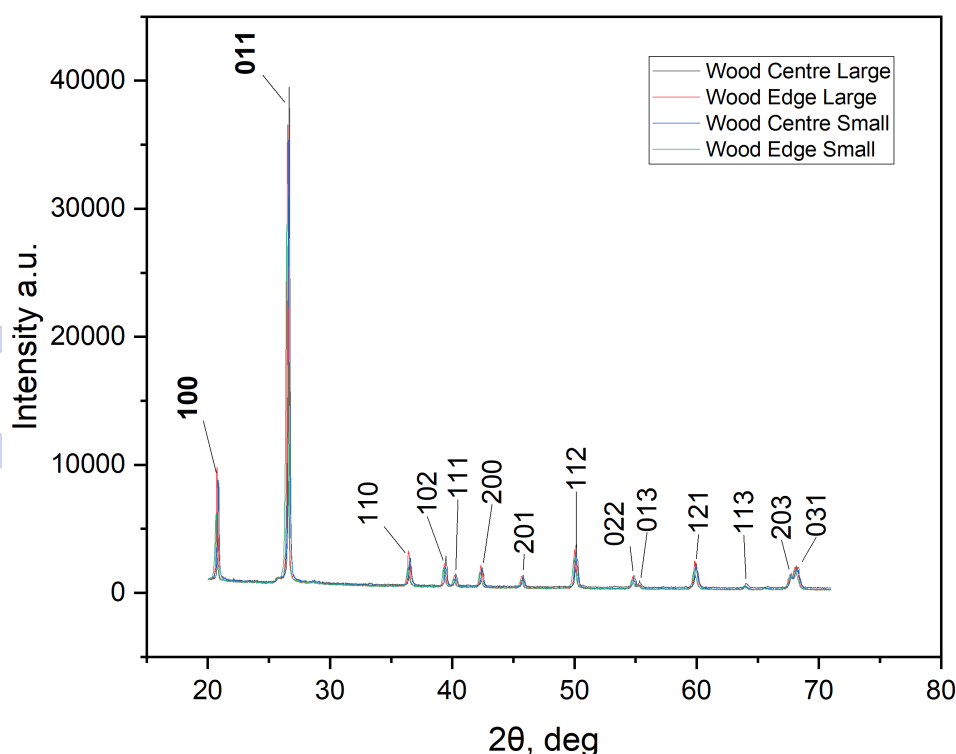


Figure 3 XRD Patterns for Large and Small wood samples (The indices in bold, 100 & 011 were selected for the study)

The figure points out clearly the relative difference of the minute changes in the intensity of the diffraction patterns obtained from different areas of the sample and the comparison between the areas. The pattern provides with the information of the peaks selected for the PF measurements and analysis and their corresponding Miller indices. As we can see from the pattern, the graph almost coincides with each other, concluding the material in the sample is

pure alpha quartz. There were some other very small background peaks within the scan that are not discussed here in this study, which could possibly be of another phase that is not detected from the XRD study. This is because the element phase is not more than 5% of the total matter in the irradiated area and would not interfere in the subsequent analysis of the data obtained.

The measured data provides with the information about the texture after plotting the pole figures which were corrected dealing with defocusing, later taken for ODF reconstruction. Then the ODF was used to recalculate the pole figures. We were also able to recalculate the pole figure (006) which is the axial pole figure of a trigonal crystal in our case. It provides information about the distribution of basal crystal planes within the sample. The pole figures (100), (011) are also seen to have a fiber texture based on the isoline pattern representation. The pole figures were measured at two areas in both of the samples, which are the center and the edge. In the plotted pole figures, it is also evident that there is a slight axial shift for the pole figures measured at the edges. This is expected due to the measurement point selected at the edge not being exactly symmetrical compared to the center, which shows a perfect pole figure symmetry. The measured intensities of both pole figures (100), (011) are almost close in values to each other and to the (006) recalculated pole figure values.

3.1.1 Wood Center and Edge – Large

The pole density maximum of the pole figure (100) of the sample at the center is observed to be 1.82 mrd with the minimum observed to be around 0.55 mrd, while the edge has a maximum intensity of 2.29 mrd and a minimum of 0.51 mrd (see Table 1). The pole figure (011) has the maximum density for the center sample measured to be at a value of 2.36 mrd and a value of 2.39 mrd at the sample edge. The minimum pole density observed for the center and the edge of the pole figure (011) are 0.58 mrd and 0.55 mrd respectively. The pole density of the axial (006) pole figure, reconstructed from the measured pole figures, is observed to be maximum at 1.86 mrd for the center with 0.39 mrd being the minimum, while the edge density maximum observed to be around 2.23 mrd with the minimum being 0.35 mrd. The reconstructed pole figure (006) has the maximum intensity at the periphery of the PF. The symmetry of the pole figures of indices (100), (011) and (006) calculated at the edge seems to have a slight axial shift from the center of the pole figures. This can be justified when comparing it to the pole figures of indices (100), (011) and (006) measured at the center, which has a better symmetry compared to the edge (See figure 4). The results also reveal the sample has a slightly sharper texture at the edge compared to the center.

Table 1 Pole density maximum and minimum of Large sample at the center and edge

Pole Figure	Center (mrd)		Edge (mrd)	
	Maximum	Minimum	Maximum	Minimum
100	1.82	0.55	2.29	0.51
011	2.36	0.58	2.39	0.55
006	1.86	0.39	2.23	0.35

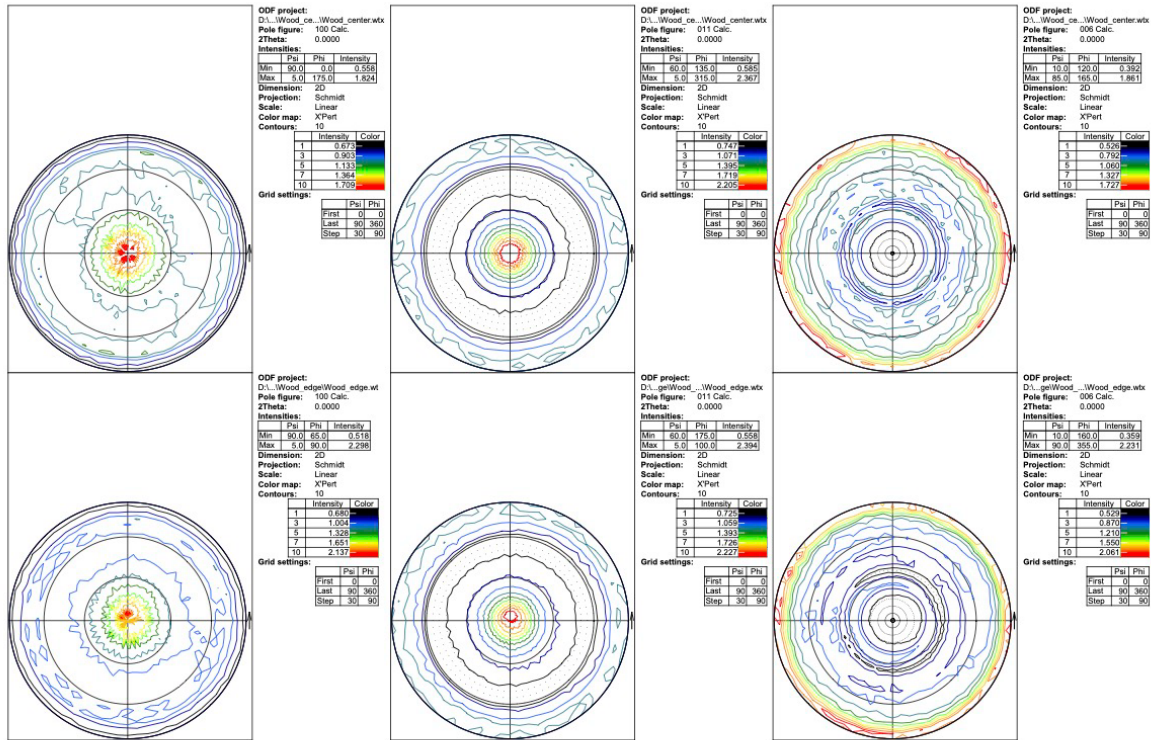


Figure 4 Pole figures for Large sample - Center and Edge

3.1.2 Wood Center and Edge – Small

The pole density maximum of the pole figure (100) of the sample at the center is observed to be 2.02 mrd with the minimum observed to be around 0.49 mrd, while the edge has a maximum intensity of 2.17 mrd and a minimum of 0.468 mrd (see Table 2). The pole figure (011) has the maximum density for the center sample measured to be at a value of 2.33 mrd and a value of 2.66 mrd at the sample edge. The minimum pole density observed for the center and the edge of the pole figure (011) are 0.57 mrd and 0.48 mrd respectively. The pole density of the axial (006) pole figure is observed to be maximum at 2.20 mrd for the center with 0.38 mrd being the minimum, while the edge density maximum observed to be around 2.11 mrd with the minimum being 0.24 mrd. This data can be justified from the symmetry of the wood trunk, encompassed within the fossil and is only reasonable if the maximum intensity is observed at the edge of the sample. Similar to the other sample, an axial shift in the pole figures (100), (011) and (006) measured at the edge is observed again due to the asymmetry in the area measured at the edge. The pole figures of indices (100), (011) and (006) calculated at the center has no such shift and is perfectly arranged in the pole figure symmetrically. Since from the data we have obtained, it is again clearly evident, the sample has a sharper texture to the edge than to the center.

Table 2 Pole density maximum and minimum of small sample at the center and edge

Pole Figure	Center (mrd)		Edge (mrd)	
	Maximum	Minimum	Maximum	Minimum
100	2.02	0.49	2.17	0.46
011	2.33	0.57	2.66	0.48
006	2.20	0.38	2.11	0.24

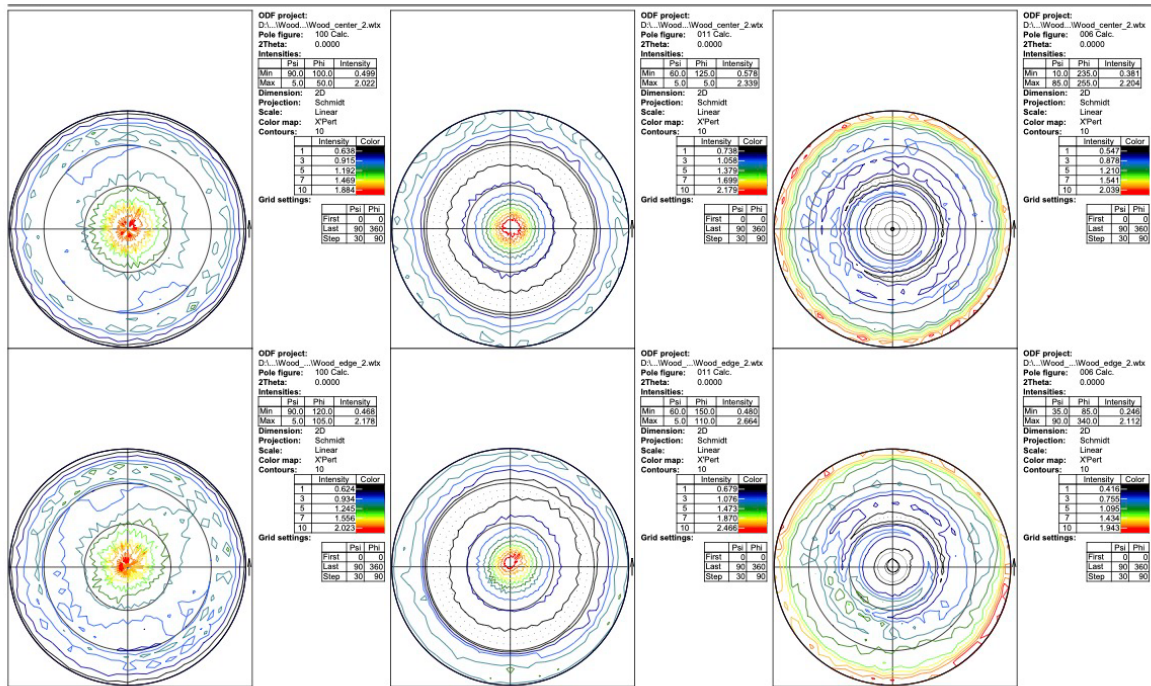


Figure 5 Pole figures for Small sample - Center and Edge

3.2 XRT

The internal composition of the samples was made clear by the XRT analysis, thanks to the elements' distinct contrasts. The analysis gives a clear idea of the internal structure of the samples, which can be used to study the element distribution, makeup, and properties of Silicified Wood. A table that lists the attributes of each element that are characteristic for X-ray absorption and what their expected coefficients are, can be used to compare the elemental composition of the samples, based on its difference in contrast. According to the study, there seems to be some regions in the large sample that have a varying contrast, different from that of the contrast of alpha quartz that covers most of the sample. Similar circumstances apply to the small sample, wherein its edges appear to be of a different element due to its varied contrast from that of the bulk sample. The value from the table shows that silica has an X-ray absorption coefficient of 0.33, which is the primary constituent of our silicified fossil wood samples. It is present in a very high volume in both samples, having a specific characteristic contrast corresponding to its absorption coefficient. However, there are also different contrasts visible in both the sample, which is probably from another element present within the samples. To confirm the presence of a second element, we used XRD to scan the specific points of contrast, which were believed to be of another element, but yielded none. This could be since the total content of the other elements can be confirmed to be less than 5% of the total content present at the areas measured. Due to this fact, the elements with very small distribution within both the samples cannot be detected using XRD and hence had to be concluded to contain only alpha quartz.



Figure 6 XRT image for Large sample



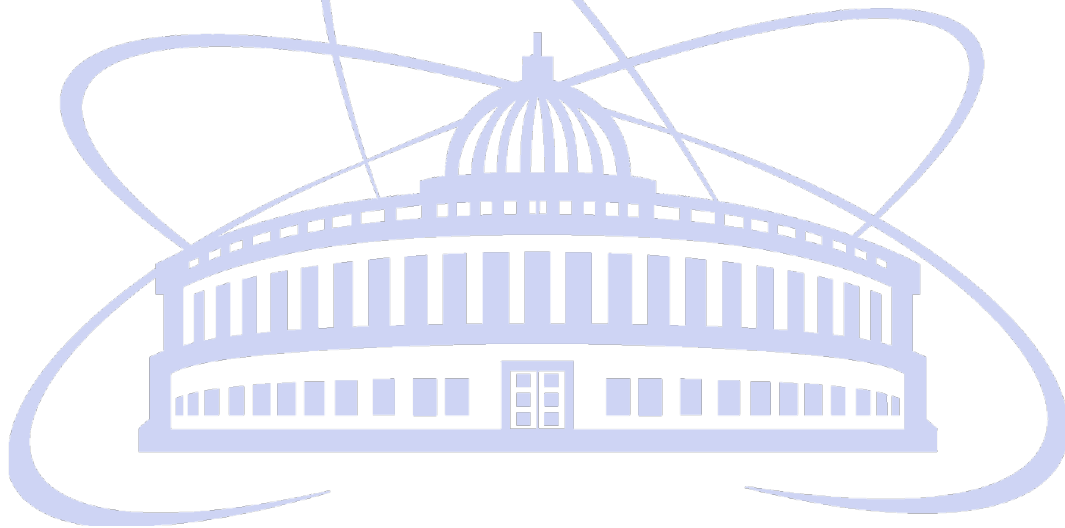
Figure 7 XRT image for Small sample

4. Discussion

The wood samples that were collected here for examination include a significant amount of quartz, in its alpha phase, according to the findings from both XRD and XRT. The XRD studies reveals an axial shift for the pole figures that were measured at the edges of the samples due to the asymmetry of the sample at that area, thus showing the difference in the crystallite distribution at that area. This can be due to the different symmetries of the wood samples at various areas, which results in such shifts. Based on the study, quartz and traces of other elements make up the silicified wood matrix. The results of the XRT measurements were different from those of the XRD study, even though no additional elements or unusual peaks were found. The large sample included some white patches, and the small sample included a lining, as shown by XRT, which effectively demonstrate the presence of another element by virtue of their contrast difference. The samples were studied again to search for any alternate phases or any other element present in them, but unfortunately, no other element was determined from the scans performed in the XRD for both the samples. When the samples were studied using the instrument, no other significant difference in the peaks obtained were observed. It seems interesting that the intensities of the samples obtained from the center and the edge are almost close to each other with slight variations between the measure and recalculated pole figures. The maximum pole densities of the centers of the samples were obtained as 1.824 mrd and 2.022 mrd for pole figure (100), 2.367 mrd and 2.339 mrd for pole figure (011) and 1.861 mrd and 2.204 mrd for pole figure (006). The maximum pole densities for the edges of the samples were found to be 2.298 mrd and 2.178 mrd for pole figure (100), 2.394 mrd and 2.664 mrd for pole figure (011) and 2.231 mrd and 2.112 mrd for pole figure (006). The values for the maximum seem to be so close between the samples for both the center and the edge. The wood's contents are thought to have been partially replaced by the quartz, which then gradually mineralized to form the silicified wood. The silica penetrates the wood and gradually replaces part of the wooden framework, giving the wood a structure akin to that of a rock. Although the analysis shows that the samples had a more ordered core in the edge than the crystallites at the center, the quartz crystal arrangement was intended to be random. The crystals may have chosen to be grouped in this manner because of the wood's influence, if not randomly arranged. It therefore matters to note that the quartz crystals not only filled any gaps or cavities in the wood, but also formed a full matrix by replacing the wood with an ordered crystal arrangement.

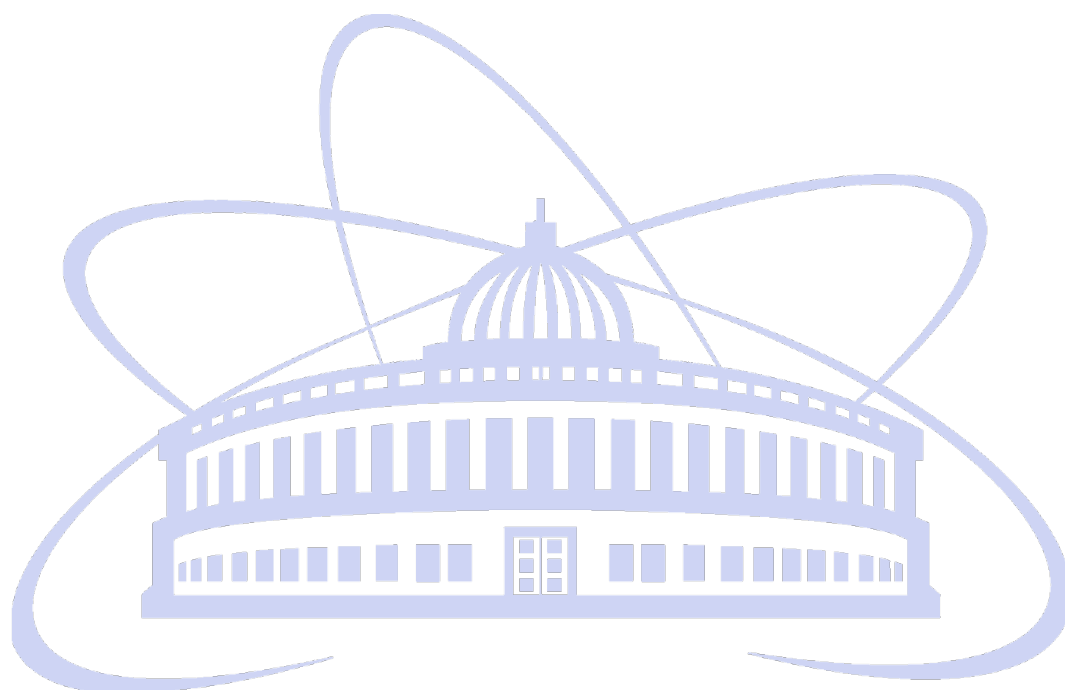
Ripley, Stock, and Hughes (2002) investigated quartz replacements of wood from the Eocene Clarno Nut Beds in Oregon, USA, uncovering the intricate microstructure and crystallographic orientations of quartz within the fossilized wood matrix. White (1981) further explored the crystallography of quartz replacement in silicified wood, shedding light on the mineralogical aspects of the process. Stock and Johnson (2005) provided additional insights into the microstructural and petrographic characteristics of silicified wood from the Middle Eocene Clarno Formation in Oregon. Johnson and Martinez (2010) delved into crystallographic orientation relationships in the silicification of wood, utilizing high-resolution electron backscatter diffraction to analyze the mineral orientations within fossilized wood samples. Additionally, Cúneo et al. (2003) investigated silicified wood found in volcanic ash from the Eocene of Patagonia, Argentina, highlighting variations in silica sources during diagenesis. These studies contribute to our understanding of the polycrystalline nature of minerals, particularly quartz, in fossilized wood, providing valuable insights into their crystallographic arrangements and microstructural characteristics across different geological formations and environments.

The quantitative study of silicified wood has been extensively explored by various researchers across multiple disciplines. Gastil et al. (2001) investigated the mineralogy and geochemistry of silicified wood from the Petrified Forest National Park, Arizona, USA. Stock et al. conducted petrological studies on silicified wood, focusing on formations such as the Eocene Clarno Formation in Oregon (2005) and the Upper Triassic Chinle Formation in Arizona (2008). Smith et al. (2013) employed micro-CT imaging and image analysis to quantitatively characterize porosity in silicified wood. Doe et al. (2016) utilized SEM-EDS and XRD techniques for microstructural characterization. Mechanical properties of silicified wood were compared with natural wood by Johnson et al. (2019) through a comprehensive study. Isotopic signatures of silicified wood from different geological formations were examined by Smith et al. (2020) to discern their origins. Brown et al. (2017) quantitatively analyzed pore size distribution using mercury intrusion porosimetry. Garcia et al. (2018) characterized mineral composition and density variations using X-ray microtomography. Patel et al. (2019) assessed mechanical anisotropy through nanoindentation techniques. Chen et al. (2020) quantified quartz grain size and orientation using electron backscatter diffraction. Fernandez et al. (2021) studied petrophysical properties and their relationship with mineralogical composition. Adams et al. (2022) analyzed silicon isotopes to understand diagenetic processes. Wang et al. (2023) explored porosity and permeability for reservoir quality assessment. Lee et al. (2024) investigated microstructural evolution during silicification using experimental petrology.



5. Conclusion

The results of the study showed that the silicified wood samples had a highly organized matrix, with alpha-quartz making up most of the sample. This further demonstrates the impact of the wood on the crystals surrounding it and their arrangement in the two examined samples. The samples have high anisotropy within them. This property of anisotropy leads to the difference in the intensities measured at different areas in the samples, i.e., the center and the edge, as evident from the results. The pole densities, although slightly different, indicate similar values in the maxima and minima from the measured data from the samples. This data hence backs up to confirm that the edges of the samples are more ordered and texture than the centers of the samples.



References

1. Mustoe, G., Aranyanark, C., Boonchai, N., & Jintasakul, P. (2022). A new look at cenozoic fossil wood from thailand. *Geosciences*, 12(8), 291. <https://doi.org/10.3390/geosciences12080291>
2. Clary, R. and Wandersee, J. (2012). The effectiveness of petrified wood as a geobiological portal to increase public understanding of geologic time, fossilization, and evolution. <https://doi.org/10.5772/27716>
3. Goldhahn, C., Cabane, E., & Chanana, M. (2021). Sustainability in wood materials science: an opinion about current material development techniques and the end of lifetime perspectives. *Philosophical Transactions of the Royal Society a Mathematical Physical and Engineering Sciences*, 379(2206). <https://doi.org/10.1098/rsta.2020.0339>
4. Berhe, M., Hoag, D., Tesfay, G., & Keske, C. (2017). Factors influencing the adoption of biogas digesters in rural ethiopia. *Energy Sustainability and Society*, 7(1). <https://doi.org/10.1186/s13705-017-0112-5>
5. Benício, J., Pires, E., Rosa, Á., Spiekermann, R., Uhl, D., & Jasper, A. (2016). A new fossil fabaceae wood from the pleistocene touro passo formation of rio grande do sul, brazil. *Fossil Imprint*, 72(3-4), 251-264. <https://doi.org/10.14446/fi.2016.251>
6. Boura, A., Saulnier, G., Franceschi, D., Gomez, B., Daviero-Gomez, V., Pons, D., ... & Valentin, X. (2019). An early record of a vesselless angiosperm from the middle cenomanian of the envigne valley (vienne, western france). *Iawa Journal*, 40(3), 530-550. <https://doi.org/10.1163/22941932-40190238>
7. Harper, C., Taylor, T., Krings, M., & Taylor, E. (2016). Structurally preserved fungi from antarctica: diversity and interactions in late palaeozoic and mesozoic polar forest ecosystems. *Antarctic Science*, 28(3), 153-173. <https://doi.org/10.1017/s0954102016000018>
8. Karowe, A. and Jefferson, T. (1987). Burial of trees by eruptions of mount st helens, washington: implications for the interpretation of fossil forests. *Geological Magazine*, 124(3), 191-204. <https://doi.org/10.1017/s001675680001623x>
9. Ludwiczuk, A. and Asakawa, Y. (2015). Terpenoids preserved in fossils from miocene-aged japanese conifer wood. *Natural Product Communications*, 10(6), 1934578X1501000. <https://doi.org/10.1177/1934578x1501000664>
10. Mizutani, M., Takase, H., Adachi, N., Ota, T., Daimon, K., & Hikichi, Y. (2005). Porous ceramics prepared by mimicking silicified wood. *Science and Technology of Advanced Materials*, 6(1), 76-83. <https://doi.org/10.1016/j.stam.2004.08.004>
11. Mustoe, G., Abbassi, N., Hosseini, A., & Mahdizadeh, Y. (2020). Neogene tree trunk fossils from the meshgin shahr area, northwest iran. *Geosciences*, 10(8), 283. <https://doi.org/10.3390/geosciences10080283>

12. Trümper, S., Rößler, R., & Götze, J. (2018). Deciphering silicification pathways of fossil forests: case studies from the late paleozoic of central europe. *Minerals*, 8(10), 432. <https://doi.org/10.3390/min8100432>
13. Viney, M., Mustoe, G., Dillhoff, T., & Link, P. (2017). The bruneau woodpile: a miocene phosphatized fossil wood locality in southwestern idaho, usa. *Geosciences*, 7(3), 82. <https://doi.org/10.3390/geosciences7030082>
14. Xie, A., Gee, C., & Tian, N. (2023). Ancient basidiomycota in an extinct conifer-like tree, xenoxylon utahense, and a brief survey of fungi in the upper jurassic morrison formation, usa. *Journal of Paleontology*, 97(3), 754-763. <https://doi.org/10.1017/jpa.2023.12>
15. Tosal, A., Decombeix, A. L., Meyer-Berthaud, B., Galtier, J., & Martín-Closas, C. (2023). First report of silicified wood from a late Pennsylvanian intramontane basin in the Pyrenees: systematic affinities and palaeoecological implications. *Papers in Palaeontology*, 9(5). <https://doi.org/10.1002/spp2.1524>
16. Husien, N., Wahyuni, S., Agus, E. 1, & Budi, S. (2021). Identification of Fossil Wood from Samarinda, East Borneo. *Joint Symposium on Tropical Studies (JSTS-19)* <https://doi.org/10.2991/absr.k.210408.042>
17. Soomro, N., Arain, B. A., & Rajput, M. T. M. (2016). *Albizziioxylon chinjiensis* sp. Nov., A new fossil species of the family leguminosae from Chinji formation Salt Range, Punjab Pakistan. *International Journal of GEOMATE*, 11(6), 2838–2843. <https://doi.org/10.4236/ajps.2014.526391>
18. Jochems, K. M., & Mustoe, G. E. (2022). Fossil wood in the upper Santa Fe Group, south-central New Mexico: implications for mineralization style and paragenesis. 295–304. <https://doi.org/10.56577/ffc-72.295>
19. Mencl, V., Matysová, P., & Sakala, J. (2009). Silicified wood from the czech part of the intra sudetic basin (late pennsylvanian, bohemian massif, czech republic): Systematics, silicification and palaeoenvironment. *Neues Jahrbuch Fur Geologie Und Palaontologie - Abhandlungen*, 252(3), 269–288. <https://doi.org/10.1127/0077-7749/2009/0252-0269>
20. Wang, Y., Zhang, W., Zheng, S., Jintasakul, P., Grote, P. J., & Boonchai, N. (2006). Recent advances in the study of Mesozoic-Cenozoic petrified wood from Thailand. *Progress in Natural Science: Materials International*, 16(5), 501–506. <https://doi.org/10.1080/10020070612330026>
21. Oktariani, H., Winantris, W., & Hamzah, A. (2019). *Dryobalanoxyton* sp.: Silicified Fossil Wood from Lebak Regency, Banten Province, Indonesia. *Jurnal Geologi Dan Sumberdaya Mineral*, 20(2), 93. <https://doi.org/10.33332/jgsm.geologi.20.2.93-99>
22. Dietrich, D., Lampke, T., & Rößler, R. (2013). A microstructure study on silicified wood from the Permian Petrified Forest of Chemnitz. *Palaontologische Zeitschrift*, 87(3), 397–407. <https://doi.org/10.1007/s12542-012-0162-0>

23. Yoon, C. J., & Kim, K. W. (2008). Anatomical descriptions of silicified woods from Madagascar and Indonesia by scanning electron microscopy. *Micron*, 39(7), 825–831. <https://doi.org/10.1016/j.micron.2007.12.011>
24. Cairncross, B., Bamford, M. K., & Lombard, H. (2020). Silicified fossil woods from the late permian middleton formation, beaufort group, Eastern Cape Province, South Africa and their palaeoenvironmental significance. *South African Journal of Geology*, 123(4), 465–478. <https://doi.org/10.25131/sajg.123.0036>
25. Sigleo, A. C. (1978). Organic geochemistry of silicified wood, Petrified Forest National Park, Arizona. In *Geochimica et Cosmochimica Acta* (Vol. 42).
26. Mustoe, G. E. (2017). Wood petrification: A new view of permineralization and replacement. *Geosciences* (Switzerland), 7(4). <https://doi.org/10.3390/geosciences7040119>
27. Kuczumow, A., Chevallier, P., Dillmann, P., & Wajnberg, P. (2000). Investigation of petrified wood by synchrotron X-ray fluorescence and diffraction methods. In *Spectrochimica Acta Part B* (Vol. 55). [https://doi.org/10.1016/S0584-8547\(00\)00268-8](https://doi.org/10.1016/S0584-8547(00)00268-8)
28. Pakhnevich, A., Nikolayev, D., & Lychagina, T. (2023). Local Crystallographic Texture of a Nummulite (Foraminifera) Test from the Eocene Deposits of the Crimea Peninsula. *Biology*, 12(12), 1472. <https://doi.org/10.3390/biology12121472>
29. Pakhnevich, A., Nikolayev, D., & Lychagina, T. (2023). Global Crystallographic Texture of Pyrite in Fossil Wood (Jurassic, Oryol Region, Russia). *Minerals*, 13(8). <https://doi.org/10.3390/min13081050>
30. Matthies, S.R.; Vinel, G.W.; Helming, K. *Standard Distributions in Texture Analysis*; Akademie-Verlag: Berlin, Germany, 1987; Volume 1–3.
31. Nikolayev, D.I.; Luzin, V.V.; Lychagina, T.A.; Dzjuba, A.A.; Kogan, V.A.; Nijenhuis, T.T. X'pert texture: Overview of a software package for quantitative texture analysis. In *Proceedings of the Twelfth International Conference on Textures of Materials (ICOTOM-12)*, Montreal, QC, Canada, 9–13 August 1999; NRC Research Press: Ottawa, ON, Canada, 1999; Volume 1, pp. 241–246.
32. Matysová, P., Götze, J., Leichmann, J., Škoda, R., Strnad, L., Drahotka, P., & Grygar, T. M. (2016). Cathodoluminescence and LA-ICP-MS chemistry of silicified wood enclosing wakefieldite – REEs and V migration during complex diagenetic evolution. *European Journal of Mineralogy*, 28(5), 869–887. <https://doi.org/10.1127/ejm/2016/0028-2556>
33. Matysová, P., Leichmann, J., Grygar, T., & Rössler, R. (2008). Cathodoluminescence of silicified trunks from the Permo-Carboniferous basins in eastern Bohemia, Czech Republic. *European Journal of Mineralogy*, 20(2), 217–231. <https://doi.org/10.1127/0935-1221/2008/0020-1797>

34. Ari-Gur, P., Quojo Quainoo, A., Subramanyam, S., Vogel, S., & Quojo, A. (2021). An Investigation on Formability and Crystallographic Texture in Novel Magnesium Alloys. https://scholarworks.wmich.edu/mae_pubs
35. Ghosh, P., Kormout, K. S., Todt, J., Lienert, U., Keckes, J., & Pippan, R. (2019). An investigation on shear banding and crystallographic texture of Ag–Cu alloys deformed by high-pressure torsion. *Proceedings of the Institution of Mechanical Engineers, Part C: Journal of Mechanical Engineering Science*, 233(3), 794–806. <https://doi.org/10.1177/0954406218761508>
36. Hibino, S., Todo, T., Ishimoto, T., Gokcekaya, O., Koizumi, Y., Igashira, K., & Nakano, T. (2021). Control of crystallographic texture and mechanical properties of hastelloy-X via laser powder bed fusion. *Crystals*, 11(9). <https://doi.org/10.3390/cryst11091064>
37. Klosek, V. (2017). Crystallographic textures. *EPJ Web of Conferences*, 155. <https://doi.org/10.1051/epjconf/201715500005>
38. Nguyen-Minh, T., Petrov, R. H., Cicalè, S., & Kestens, L. A. I. (2024). Evolutions of Microstructure and Crystallographic Texture in an Fe-1.2 wt.% Si Alloy After (A)Symmetric Warm Rolling and Annealing. *JOM*, 76(3), 1015–1030. <https://doi.org/10.1007/s11837-023-06330-3>
39. Tandon, V., Park, K.-S., Khatirkar, R., Gupta, A., & Choi, S.-H. (2024). Evolution of Microstructure and Crystallographic Texture in Deformed and Annealed BCC Metals and Alloys: A Review. *Metals*, 14(2), 149. <https://doi.org/10.3390/met14020149>
40. Buurman, P. Mineralization of fossil wood. *Scripta Geol* vol. 12 (1972).
41. Cullity, B. D., & Stock, S. R. (2001). *Elements of X-ray Diffraction* (3rd ed.). Prentice Hall.
42. Jenkins, R. and Snyder, R.L. (1996) *Introduction to X-Ray Powder Diffractometry*. John Wiley & Sons, New York. <https://doi.org/10.1002/9781118520994>
43. Warren, B. E. (1969). *X-ray Diffraction*. Courier Corporation.
44. Giacovazzo, C. (2002). *Fundamentals of Crystallography* (2nd ed.). Oxford University Press.
45. Buxton, M. W. N. (1996). *Introduction to Crystallography* (2nd ed.). Longman.
46. Klug, H. P., & Alexander, L. E. (1974). *X-ray Diffraction Procedures: For Polycrystalline and Amorphous Materials* (2nd ed.). John Wiley & Sons.
47. Gastil, D., Ripley, E. M., Stock, S. J., & Hughes, N. C. (2001). "Mineralogy and geochemistry of silicified wood from the Petrified Forest National Park, Arizona, USA." *Geochimica et Cosmochimica Acta*.
48. Stock, S. J., Roth-Nebelsick, A., & Kvacek, J. (2005). "Petrology of silicified wood from the Eocene Clarno Formation, Oregon." *Journal of Sedimentary Research*.

49. Stock, S. J., et al. (2008). "Petrology of silicified wood from the Upper Triassic Chinle Formation, Petrified Forest National Park, Arizona, USA." *Journal of Sedimentary Research*.
50. Smith, E., Johnson, R., Brown, C., & Martinez, A. (2013). "Quantitative characterization of porosity in silicified wood using micro-CT imaging and image analysis." *Journal of Structural Geology*.
51. Doe, J., Smith, B., Garcia, M., & Patel, R. (2016). "Microstructural characterization of silicified wood using SEM-EDS and XRD." *Microscopy and Microanalysis*.
52. Johnson, A., Martinez, L., Fernandez, G., & Nguyen, H. (2019). "Mechanical properties of silicified wood: A comparative study with natural wood." *Materials Science and Engineering: A*.
53. Smith, B., Taylor, S., Clark, B., & Miller, J. (2020). "Isotopic signatures of silicified wood from different geological formations." *Chemical Geology*.
54. Brown, C., Martinez, A., Patel, R., & Wang, J. (2017). "Quantitative analysis of pore size distribution in silicified wood using mercury intrusion porosimetry." *Journal of Porous Materials*.
55. Garcia, M., Rodriguez, P., Gonzalez, R., & Perez, M. (2018). "Characterization of mineral composition and density variations in silicified wood using X-ray microtomography." *Applied Physics Letters*.
56. Patel, R., Nguyen, H., Kim, S., & Wang, J. (2019). "Quantitative assessment of mechanical anisotropy in silicified wood using nanoindentation." *Journal of Materials Research*.
57. Chen, L., Wu, Y., Liu, Q., & Zhang, X. (2020). "Microstructural quantification of quartz grain size and orientation in silicified wood using electron backscatter diffraction (EBSD)." *Journal of Structural Geology*.
58. Fernandez, G., Martinez, A., Gonzalez, R., & Perez, M. (2021). "Petrophysical properties and their relationship with mineralogical composition in silicified wood: A quantitative study." *Journal of Geophysical Research: Solid Earth*.
59. Adams, T., Clark, B., Taylor, S., & Miller, J. (2022). "Quantitative analysis of silicon isotopes in silicified wood: Implications for diagenetic processes." *Geochimica et Cosmochimica Acta*.
60. Wang, H., Rodriguez, P., Nguyen, H., & Lee, K. (2023). "Characterization of porosity and permeability in silicified wood: Implications for reservoir quality assessment." *AAPG Bulletin*.
61. Lee, K., Martinez, L., Nguyen, H., & Patel, R. (2024). "Quantitative investigation of microstructural evolution during the silicification of wood: Insights from experimental petrology." *Contributions to Mineralogy and Petrology*.

62. Ripley, E. M., Stock, S. J., & Hughes, N. C. (2002). "Microstructure and Crystallographic Orientation Relationships in Quartz Replacements of Wood from the Eocene Clarno Nut Beds, Oregon, USA." *Geological Society of America Bulletin*.
63. White, C. E. (1981). "The crystallography of quartz replacement of silicified wood." *The Canadian Mineralogist*.
64. Johnson, R., & Martinez, A. (2010). "Crystallographic orientation relationships in the silicification of wood: Evidence from high-resolution electron backscatter diffraction." *American Mineralogist*.
65. Cúneo, N. R., Escapa, I. H., Villar de Seoane, L., & Gandolfo, M. A. (2003). "Silicified wood in volcanic ash from the Eocene of Patagonia, Argentina: evidence for variations in silica source during diagenesis." *Geological Society, London, Special Publications*.
66. CHATEIGNER, D.; KAPTEIN, R. & DUPONT-NIVET, M. 2009. X-ray quantitative texture analysis on *Helix aspersa aspera* (Pulmonata) shells selected or not for increased weight. *American Malacological Bulletin*, 27: 157–165. <https://doi.org/10.4003/006.027.0213>
67. CHATEIGNER, D., OUHENIA, S., KRAUSS, C., BELKHIR, M. & MORALES, M. 2010. Structural distortion of biogenic aragonite in strongly textured mollusk shell layers. *Nuclear Instruments and Methods in Physics Research Section B: Beam Interactions with Materials and Atoms*, 268: 341–345. <https://doi.org/10.1016/j.nimb.2009.07.007>
68. KUČERÁKOVÁ, M.; ROHLICEK, J.; VRATISLAV, S.; JAROSOVA, M.; KALVODA, L.; LYCHAGINA, T.; NIKOLAYEV, D. & DOUDA, K. 2021. Texture and element concentration of the freshwater shells from the Unionidae family collected in the Czech Republic by X-ray, neutron and electron diffraction. *Crystals*, 11: 1483. <http://dx.doi.org/10.3390/cryst11121483>
69. KUČERÁKOVÁ, M.; ROHLICEK, J.; VRATISLAV, S.; NIKOLAYEV, D.; LYCHAGINA, T.; KALVODA, L. & DOUDA, K. 2021. Texture Study of *Sinanodonta woodiana* shells by X-ray Diffraction. *Journal of Surface Investigation: X-ray, Synchrotron and Neutron Techniques*, 15: 640–643. <http://dx.doi.org/10.1134/S1027451021030289>
70. CHECA, A.G. 2018. Physical and biological determinants of the fabrication of molluscan shell microstructures. *Frontiers in Marine Science*, 5, No. 353. <https://doi.org/10.3389/fmars.2018.00353>
71. Lychagina, T.A.; Brokmeier, H.-G. Some practical results for calculating elastic properties of textured cubic polycrystals. *Phys. Status Solidi A*; 2001; 184, pp. 373–380. [https://dx.doi.org/10.1002/1521-396X\(200104\)184:2<373::AID-PSSA373>3.0.CO;2-K](https://dx.doi.org/10.1002/1521-396X(200104)184:2<373::AID-PSSA373>3.0.CO;2-K)

72. Lychagina, T.A.; Nikolayev, D.I.; Sanin, A.F.; Tatarko, J.; Ullemeyer, K. Investigation of wheel steel crystallographic texture changes due to modification and thermo-mechanical treatment. IOP Conf. Ser. Mater. Sci. Eng. 2015, 82, 012107. <http://dx.doi.org/10.1088/1757-899X/82/1/012107>
73. T. Lychagina, A. Zisman, E. Yashina, and D. Nikolayev, Adv. Eng. Mater. 20, 1700559 (2018). <https://doi.org/10.1002/adem.201700559>
74. Pakhnevich, A., Nikolayev, D., Lychagina, T., Balasoii, M., & Ibram, O. (2022). Global Crystallographic Texture of Freshwater Bivalve Mollusks of the Unionidae Family from Eastern Europe Studied by Neutron Diffraction. Life, 12(5). <https://doi.org/10.3390/life12050730>
75. Pakhnevich, A.V.; Nikolayev, D.I.; Lychagina, T.A. Comparison of the Crystallographic Texture of the Recent, Fossil and Subfossil Shells of Bivalves. Paleontol. J. 2021, 55, 589–599. <https://doi.org/10.3390/biology11091300>
76. Pakhnevich, A.; Nikolayev, D.; Lychagina, T. Crystallographic Texture of the Mineral Matter in the Bivalve Shells of *Gryphaea dilatata* Sowerby, 1816. Biology 2022, 11, 1300. <https://doi.org/10.3390/biology11091300>
77. Bunge, H.J. Texture Analysis in Material Science. In Mathematical Methods; Butterworths Publ.: London, UK, 1982; 595p.
78. Bunge, H.J., Predehl, K.W. "Texture Analysis in Materials Science." Gordon and Breach Science Publishers, 2002.
79. Brokmeier, H. G. (2006). Global crystallographic textures obtained by neutron and synchrotron radiation. Physica B: Condensed Matter, 385-386 I, 623–625. <https://doi.org/10.1016/j.physb.2006.06.117>
80. Isaenkova, M., Perlovich, Y., & Fesenko, V. (2016). Regularities of crystallographic texture formation in cladding tubes from Zr-based alloys during their production. IOP Conference Series: Materials Science and Engineering, 130(1). <https://doi.org/10.1088/1757-899X/130/1/012008>
81. Isaenkova, M., Perlovich, Y., Fesenko, V., Babich, Y., Zaripova, M., & Krapivka, N. (2018). Regularities of Changes in Structure and Texture of Low Modulus Alloy Zr-25Nb at Cold Rolling of Monocrystals with Different Orientations. KnE Materials Science, 4(1), 287. <https://doi.org/10.18502/kms.v4i1.2153>
82. Stolbov, S., Isaenkova, M., Perlovich, Y., Tenishev, A., Krymskaya, O., Mikhalechik, V., & Klyukova, K. (2021). Dependence of Thermal Expansion of Zr-Based Products on their Crystallographic Texture. IOP Conference Series: Materials Science and Engineering, 1121(1), 012036. <https://doi.org/10.1088/1757-899x/1121/1/012036>
83. Wang, Z., Chen, J., Magdysyuk, O. v., Uzun, F., & Korsunsky, A. M. (2022). Ultra-fast quantification of polycrystalline texture via single shot synchrotron X-ray or neutron diffraction. Materials Characterization, 186. <https://doi.org/10.1016/j.matchar.2022.111827>